Aalborg Universitet

[Link to publication from Aalborg University](#)

Measurement of bubble shape and size in bubbly flow structure for stagnant and pulsating liquid flow using an undivided electrochlorination cell and Telecentric Direct Image Method

Nikolaj K. Andersen[1], Rodica-Elisabeta Stroe[1], Lau Hedensted[1], Anders C. Olesen[2], Jakob Hærvig[2] and Henrik Sørensen[2]

[1]*Thermal Energy And Process Engineering, School of Engineering and Science, Aalborg University*
Fibigerstræde 10, 9220 Aalborg East, Denmark
nkan11@student.aau.dk

[2]*Department of Energy Technology, Aalborg University*
Pontoppidanstræde 111, 9220 Aalborg East, Denmark
aco@et.aau.dk

Abstract

This study presents the measurement of shape and diameter of bubbles in different regions of the bubbly flow structure at the cathode for stagnant and pulsating liquid flow in a single undivided electrochlorination cell. The cell is filled with a dilute sodium chloride electrolyte solution with a concentration of 30 g/L, and operated at a current density of 18.75 mA/cm^2, and stagnant liquid flow, or pulsating liquid flow with a pulsation period of 3.5 s and rate of 760 mL/h. Measurements are conducted using a Telecentric Direct Image Method for acquiring images of the bubbles, and processing is done in MATLAB and NI Vision in LabVIEW to determine shape and diameter of the bubbles. Three bubble regions are observed: adherence, bubble diffusion and bulk region. For stagnant liquid flow the mean bubble diameter increases from 30 to 60 μm going from the adherence region to the bulk region, which is supported by an increase in fraction of total gas volume constituted by large bubbles. For pulsating liquid flow the mean bubble diameter is observed to remain constant around 35 μm when moving across the bubbly flow structure, which likewise is supported by the fraction of total gas volume investigations. Hence, showing horizontal displacement of the three bubble regions with the pulsating liquid flow.

Keywords: Direct imaging, electrochlorination, bubbly flow, bubble size, bubble shape, pulsating liquid flow

1. Introduction

Chlorine is widely used in the water treatment industry, but due to handling risks and hazards, attention has been given to on-site generation in recent years [1, 2]. Electrochlorination cells are devices for on-site hypochlorite generation through salt water electrolysis. Much research has been done experimentally, however fundamental knowledge of the processes occurring are still lacking, hence modelling of the electrochlorination process is necessary for studying the details of the process [2]. The multiphase flow behaviour is an important part of the working principle of the cell. Thus, in order to fully understand the multiphase flow behaviour in such cells, without time expensive resolving of all bubbles numerically, accurate measurements of the bubbles generated at the electrodes are required.

1.1. Measurement and visualisation technique

Many different techniques have been deployed for measuring parameters and visualising phenomena of importance in understanding multiphase flows and the influence of these on the performance of devices and processes. Such phenomena and parameters include flow regime, phase velocity and volume fraction, and bubble diameter distribution.

Bubble diameter and shape as well as flow regime and structure are of great importance since these influence the performance of electrochemical cells. Thus, to obtain these parameters and visualise the flow behaviour, imaging techniques are often used since these do not disturb the flow occurring in the cells.

1.2. Studied hydrodynamic aspects in electrochemical cells

Flow regimes have been studied intensively because generation of bubbles greatly influences the performance of electrochemical cells by hindering the liquid reactants access to the electrode surface [3]. Studies show that bubbly flow is the predominant flow regime in these electrochemical cells, but that transition to slug flow may occur at low liquid flow rates and sufficiently high current densities [3].

Several studies have been conducted on investigating bubble evolution and diameter while varying the current density. It has been seen that increasing the current density increases the bubble generation, in accordance with Faraday's law of electrolysis [3, 4, 5]. As the current density is increased, the mean bubble diameter is seen to increase [3, 6, 7, 8]. Additionally, the mean bubble diameter has been reported to increase in the direction of the flow along the electrode surface [6, 8, 9].

In the bubbly flow, the two phase flow structure occurring has been studied. It has been reported that bubbly flows consist of three regions: adherence, bubble diffusion and bulk region [6]. Furthermore, it was observed that the bubble diameter increases from the adherence region to the bulk region [6]. In the adherence region bubbles stick to or stay close to the electrodes and the thickness of this region is that of the mean diameter of the bubbles. Furthermore, the bubble diameter has been observed to increase along the flow direction in the adherence and bubble diffusion regions [6]. The larger bubbles formed through this growth have been seen to jump from the surface through bursts and into the bulk region along with smaller bubbles they had taken with them during the jump [6]. Quite dispersed bubbles were seen in the bulk region and these bubbles were not observed to grow further in size [6]. In all cases of increasing bubble diameters described in the above, the bubble growth is reported to be caused by coalescence between larger and smaller bubbles, especially in the vicinity of the electrode surface [6], and/or mass transfer from supersaturated zones in the liquid phase [8].

The present study aims at investigating bubble diameter and shape in the adherence, bubble diffusion and bulk regions oc-

curring at the electrode surfaces, under the influence of a pulsating liquid flow. In order to observe the influence of this pulsating flow, a reference investigation is performed in a stagnant liquid flow. Here stagnant liquid flow denotes an inlet velocity of zero for the electrolyte. The above is done using an undivided electrochlorination cell and Telecentric Direct Image Method (TDIM). Such investigations should be performed in the cell gap, however preliminary tests have shown low visibility between the electrodes. Hence, the investigations are carried out by studying the bubble regions above the cathode of the electrochlorination cell since this is the electrode with the predominant bubble generation.

2. Methodology

The TDIM applied in this study involves the capture of images of bubbles and subsequent analysis with the purpose of determining bubble diameter and shape. Thus TDIM enables a clear identification of the bubbles evolving at the cathode, without affecting the fluid dynamics of the system.

2.1. Experimental setup

Figure 1 shows the experimental setup which consists of an undivided electrochlorination cell, a camera, and a LED chipset with camera optics. The electrochlorination cell, with internal dimensions of 40 x 40.4 x 111 mm, is made of plexiglass and fitted with two 40 x 40 mm titanium electrodes with a cell gap of 7.5 mm. The cell has an inlet at the bottom through which the electrolyte enters and an outlet at the top through which the waste solution and the formed gases leave the cell. The electrolyte is a dilute sodium chloride solution with a concentration of 30 ± 0.1 g/L and flow rate of 760 mL/h. The inlet pressure is delivered by a Grundfos DDA 7.5-16 dosing pump with a stroke volume of 0.74 ml, which gives a pulsation period of approximately 3.5 s. The cell is operated at a constant current density of approximately 18.75 mA/cm^2 corresponding to a cell voltage of 2.5 V.
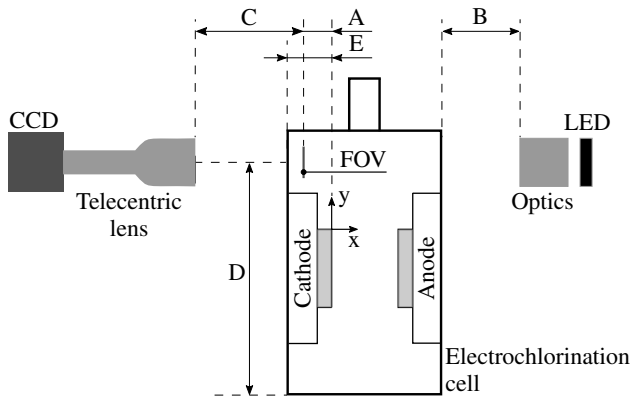

Figure 1: Conceptual drawing of the experimental setup.

The camera is a Basler acA1300-30um USB 3.0 area scan, monochrome CCD camera fitted with an Edmund Optics 63-729 telecentric lens with a 0.5x primary magnification and a working distance (C) of 110 mm. The image resolution of 1280 x 960, sensor pixel size of 3.75 x 3.75 mm and the primary magnification give the system a field of view (FOV) of 9.6 x 7.2 mm. Based on these characteristics, the camera and the optics system yield a pixel size of 7.5 μm. The FOV is located above the cathode at a height (D) of 111.2 mm and with a distance (A) to the plane of the cathode face. The cathode face is located at a distance (E) of 16.18 mm from the inner cell wall. Test are performed by moving across the bubbly flow structure from the normalised horizontal position A/E = -0.35 to A/E = -0.06, hereafter referred to as

horizontal position (A/E). The cell and the equipment described above are mounted together on a heavy aluminium structure in order to stabilize the viewing field.

As the bubbles move through the FOV of the imaging system, it is of high importance to reduce perspective, and hence measurement errors. To eliminate perspective errors occurring in the case of conventional lenses used for capturing moving objects, a telecentric lens is chosen. This lens type has a constant, zero angular FOV. Hence, a telecentric lens has a constant magnification and FOV regardless of the distance to the object [10].

The background lighting is provided by a LED chipset mounted together with camera optics. The lighting is placed at a distance (B) of 132.9 to 137.5 mm from the outer surface of the cell, when moving across the bubbly flow structure, and centred with respect to the camera and lens configuration at the height (D). This LED and camera optics combination enables focused lighting at varying intensities.

2.2. Image acquisition settings

For each image series, 100 images are captured at an exposure time of 16 μs. Preliminary measurements showed a minimum bubble velocity of approximately 1 mm/s, hence a dead time of 10 s is set between the capture of each image. This ensures that the same bubbles are not captured across multiple images and therefore do not appear multiple times in the data set. Noting that the pulsation period of 3.5 s does not align with the dead time, the dead time results in a time averaging of the captured bubbly flow structure. Hence, giving an offset of 30 seconds over 100 images.

Furthermore, each image series has a total acquisition time of 16.5 minutes per image series and a total of 10 image series are made.

2.3. Image processing and analysis

The image processing procedure is conducted in two parts; 1) Preprocessing in MATLAB and 2) Processing and analysis using the NI Vision toolbox in LabVIEW. The steps of each part is summarized in Fig. 2.

Figure 3 shows a typical unprocessed image, which includes both in-focus bubbles, with sharp contours and steep greyscale gradients, and out-of-focus bubbles, with soft edges and small greyscale gradients.

The purpose of the preprocessing is to ease the processing in LabVIEW by creating a uniform background, as well as increase the contrast between background and the bubble contours.

The first step of the preprocessing is the removal of the non-uniform background seen in Fig. 3. To do this, the original image is divided by an averaged background image and all results above 1 are set to 1, according to Eqn (1).

$$I_f(x,y) = \frac{I_0(x,y)}{\bar{I}_{BG}(x,y)} \quad \text{if } I_f > 1 \text{ then } I_f = 1 \tag{1}$$

where I_f is the foreground image (without background), I_0 is the original unprocessed image and $\bar{I}_{BG}$ is the averaged background image, which is generated by computing the average of 50 subsequently captured images with the light source on, but the cell turned off. In Eqn (1) values above 1 are set equal to 1 in order to avoid distorting the normalisation. This normalisation, shown in Eqn (2), is then applied to I_f to increase the utilization of the greyscale spectrum.

$$I_n(x,y) = \frac{I_f(x,y) - \min(I_f)}{\max(I_f) - \min(I_f)} \tag{2}$$

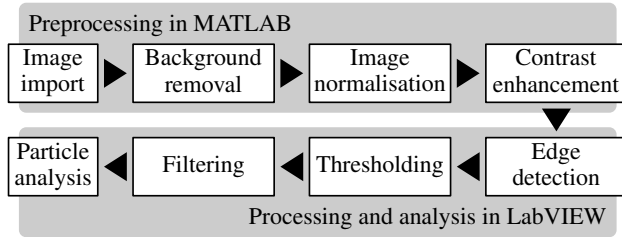where I_n is the normalised foreground image.

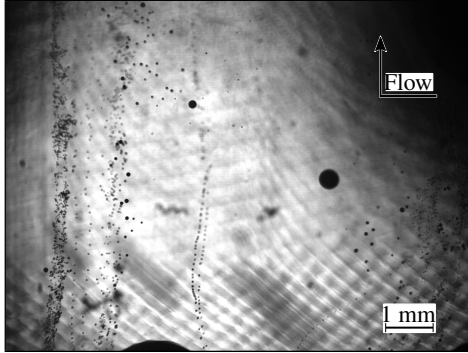Figure 2: Flowchart of the image processing procedure.

Figure 3: Unprocessed reference image of the two-phase flow.

Then, I_n undergoes contrast enhancement, which increases the greyscale values larger than 0.5 and decreases those smaller than 0.5, hence dark regions are darkened and light regions are lightened [11]. In this study a non-linear intensifier operation, given in Eqn (3), is applied for the contrast enhancement [11].

$$I_c(x,y) = \begin{cases} 2 \cdot [I_n(x,y)]^2 & \text{for } I_n \in [0.0; 0.5] \\ 1 - 2 \cdot [1 - I_n(x,y)]^2 & \text{for } I_n \in]0.5; 1.0] \end{cases} \quad (3)$$

where I_c is the contrast enhanced image. From Fig. 4 it is seen that the image preprocessing has enhanced the quality of the image in terms of bubble recognition - the uneven background has been removed and a larger contrast, and hence greyscale gradients, between particle edges and background has been created, thus, improving the conditions for edge detection.
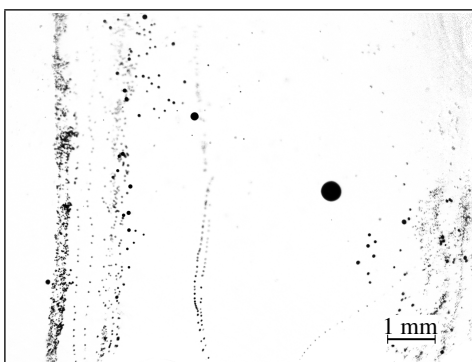

Figure 4: Reference image after preprocessing.

The preprocessed images are further processed and analysed in LabVIEW to determine bubble shape and diameter. This part of the processing aims to remove problematic bubble contours and shapes which alter the accuracy of the measurements, such as bubbles that are out of focus, have incomplete edges or overlap other bubbles. Bubble contours are extracted and outlined by means of an edge detection filter implemented in LabVIEW. The filter applied in this study is the non-linear Roberts filter, which gives in-focus bubbles with sharp edges light and complete outlines, whereas out-of-focus bubbles receive fuzzy, darker or even incomplete outlines. Afterwards a threshold of 80 is applied, which breaks up the fuzzy outlines of out-of-focus bubbles while keeping the outlines of in-focus bubbles closed and intact. The complete contours are then filled and the images go through binary morphology, which includes removal of border objects as well as single pixel sized residue. Furthermore, a ratio of equivalent ellipse axes filter excluding ratios larger than 1.5 is applied in order to remove any incomplete contours left over by the thresholding, as well as overlapping bubbles.

After the processing of the images the bubbles are analysed and bounding rectangle width, which approximates the bubble diameter, and a Heywood Circularity Factor (HCF) are extracted for each bubble. The HCF is defined as the perimeter P of the object divided by the circumference of a circle with the same area A, see Eqn (4). Thus, the closer the shape of an object is to a perfect circle, the closer the HCF is to 1.

$$\text{HCF} = \frac{P}{4\pi A} \quad (4)$$

2.4. Method verification

The TDIM was verified by applying it to polyamid particles, with a known mean size of 50 µm, suspended in water. A series of 100 images was captured and processed using the procedure described above resulting in a total of 1342 recognised and measured particles. The size distribution is shown in Fig. 5.
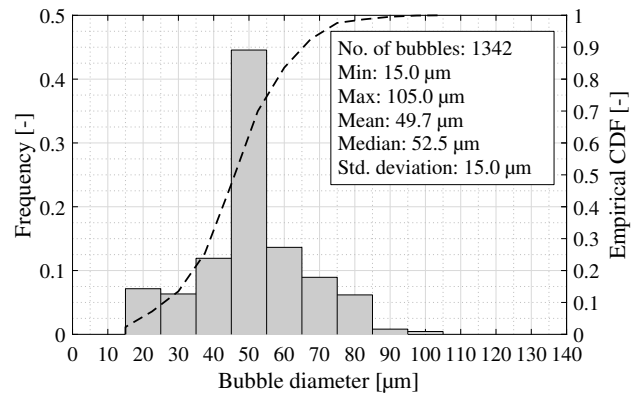
Figure 5: Normalised size distribution of polyamid particles measured using TDIM. The particles have a known mean of 50 µm.

The resulting mean estimate of 49.7 µm, with a confidence interval of approximately $\pm$ 0.9 µm, is in agreement with the known diameter of 50 µm. Thus, it is concluded that the applied method is suitable for measuring diameter and shape of bubbles evolving at the electrodes of the electrochlorination cell.

In the above a threshold of 80 was applied in the image processing. The value of the threshold influences which particles (or bubbles) are included in the final data set and which are not. In order to investigate the influence of the threshold, the processing of the polyamid particle images was repeated with thresholds of 70 and 90. The resulting mean size estimates are listed in Table 1 with the results for a threshold of 80.

From Table 1 it is seen that changing the threshold by $\pm$ 10 results in an insignificant change of the mean size estimate of approximately $\pm$ 3 %, compared to the mean size estimate with a threshold of 80.

Table 1: Estimated mean particle size and number of recognised particles for image processing thresholds of 70, 80, and 90.

Threshold	Estimated mean size [µm]	No. of particles
70	51.2	1701
80	49.7	1342
90	48.2	1065

3. Results

Figure 6 shows the HCF as function of the bubble diameter for bubbles in pulsating and stagnant liquid flow, across all investigated horizontal positions (A/E).
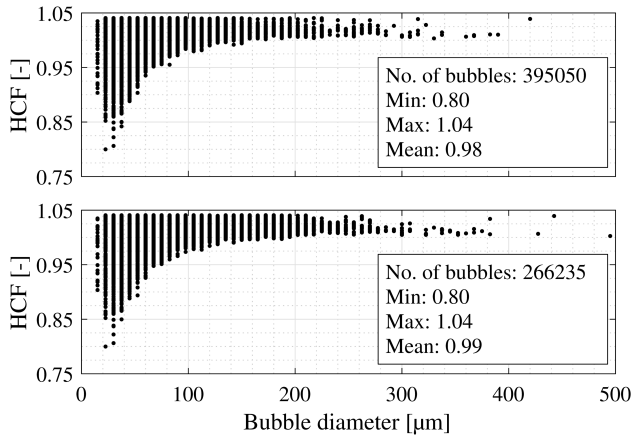

Figure 6: Heywood circularity factor measurements across all horizontal positions (A/E) for pulsating liquid flow (top) at 760 mL/h and stagnant liquid flow (bottom), 18.75 mA/cm^2, 2.5 V, and a salt concentration of 30 g/L.

As seen from Fig. 6 the mean circularity factors for both pulsating and stagnant liquid flow show that the bubbles can be considered spherical and hence the width of the bubbles is regarded as the diameter of the bubbles. Moreover, it is seen that the main portion of the bubbles are located around a circularity factor of 1, which indicates that a large portion are spherical or very close to being spherical. However, Fig. 6 also shows that smaller bubbles have circularity factors as low as 0.8 and hence appear less spherical in the data set.

Figure 7 shows a typical picture of the bubbly flow structure occurring just above and in the plane perpendicular to the cathode of the electrochlorination cell.
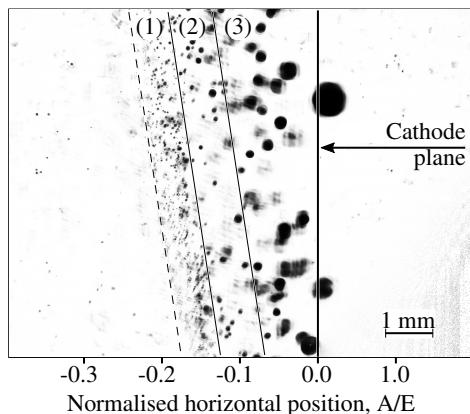

Figure 7: Bubbles above and in the plane of the cathode at 760 mL/h, 37.5 mA/cm^2, 2.8 V and a salt concentration of 30 g/L.

In Fig. 7 small bubbles seem to be confined to the left in the picture, thus being the bubbles coming from the region closest to the electrode surface to which they have been reported to adhere or stay close to. Furthermore, it is seen that the bubble diameter increases going from left to right in the picture and that dispersed large bubbles are seen in the bulk region (3) of the flow. This confirms the observations made by Ref. [6], thus showing the occurrence of three regions in the bubbly flow structure: adherence, bubble diffusion and bulk region as indicated in Fig. 7 by (1), (2) and (3), respectively. Finally, it is seen from Fig. 7 that a larger number of small bubbles are found in comparison to the number of large bubbles.

Figure 8 shows the evolution in mean bubble diameter as a function of the horizontal position (A/E) in the electrochlorination cell. The values are given with a maximum confidence interval of ± 1.1 µm.
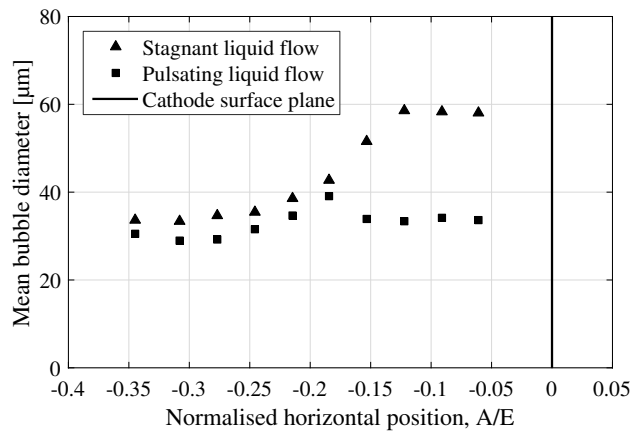

Figure 8: Mean bubble diameter as function of horizontal position (A/E) for stagnant liquid flow and pulsating liquid flow of 760 mL/h, both performed at 18.75 mA/cm^2, 2.5 V and a salt concentration of 30 g/L.

In the case of a stagnant liquid flow, Fig. 8 shows a significant increase in mean diameter of the bubbles as the horizontal position increases from -0.35 to -0.06. In the case of a pulsating flow only small variations exist in the mean bubble diameter as the horizontal position increases, and a maximum diameter difference of 10 µm is seen between A/E = -0.35 and A/E = -0.18. This is expected considering the time averaging of the bubble diameters occurring between the three regions of the bubbly flow structure. Comparing the mean bubble diameter for the stagnant and pulsating liquid flows at the different horizontal positions, it is seen that reasonable agreement exists between the mean bubble diameters at horizontal positions from -0.35 to -0.18. For A/E greater than -0.18 the mean bubble diameters are seen to deviate from each other. Moving from the adherence region (1) to the bulk region (3) means that small bubbles should move out of focus and large bubbles into focus, whereby the recognised number of small and large bubbles should decrease and increase, respectively.

Figures 9 and 10 show the fraction of total gas volume as function of bubble diameter for stagnant and pulsating liquid flow, respectively, at horizontal positions (A/E) of -0.35, -0.18 and -0.06.

As seen from Fig. 9 the fraction of total gas volume for small and large bubbles decreases and increases, respectively, as A/E goes to zero. This indicates that more small and large bubbles have moved out of and into focus, respectively, as the horizontal position increases. From Fig. 10 it is seen that the fraction of total gas volume for small and large bubbles decreases and increases, respectively, at a horizontal position of -0.18 compared to a hor-

izontal position of -0.35 as expected from Fig. 9. However, at a horizontal position of -0.06 the reverse trends with little to no large bubbles are seen.
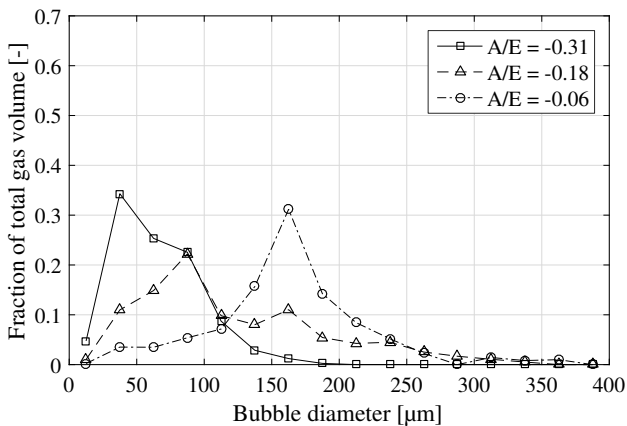

Figure 9: Fraction of total gas volume as function of bubble diameter at horizontal positions (A/E) of -0.35, -0.18 and -0.06 for stagnant liquid flow at 18.75 mA/cm^2, 2.5 V, and a salt concentration of 30 g/L.
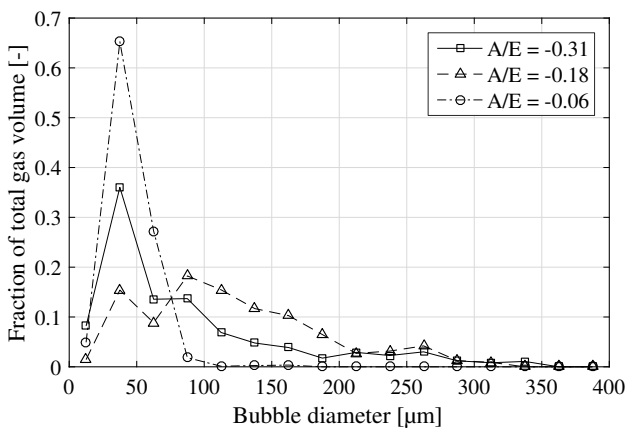

Figure 10: Fraction of total gas volume as function of bubble diameter at horizontal positions (A/E) of -0.35, -0.18 and -0.06 for pulsating liquid flow at 760 mL/h, 18.75 mA/cm^2, 2.5 V, and a salt concentration of 30 g/L.

4. Discussion

In terms of bubble shape, it is seen that the HCF of the bubbles concentrates around 1. However, the factor can go as low as 0.8 for small bubbles, as shown in Fig. 6. This is expected to be caused by small bubbles only consisting of a few pixels. Hence, a bubble can have an unclear edge, if the bubble is slightly out of focus or light reflections within the cell affecting the bubble. Thus, a pixel can be lost in the height or width of the bubble, thus skewing the shape of the bubble and make it appear non-spherical.

For stagnant liquid flow it is observed that the mean bubble diameter increases as the horizontal position increases as shown in Fig. 8. This is further supported by the fraction of total volume as function of bubble diameter, illustrated in Fig. 9, where the fraction of total gas volume of small and large bubbles decrease and increase, respectively, as the horizontal position in the cell is increased. Hence, indicating that small bubbles have

moved out of focus and large bubbles into focus. These observations are in line with the bubbly flow structure shown in Fig. 7, where the diameter of the bubbles are seen to increase moving from the adherence region (1) to the bulk region (3).

For pulsating liquid flow small variations in mean bubble diameters as function of horizontal position are observed, where only a difference in bubble diameter of 10 μm is found. These small variations are further supported by the fraction of total gas volume as function of bubble diameter, as illustrated in Fig. 10, where the fraction of total gas volume for small and large bubbles decrease and increase, respectively, up to a horizontal position (A/E) of -0.18 after which the reverse trend is observed. These observations are inconsistent with the bubbly flow structure shown in Fig. 7. Hence, indicating that small and large bubbles move across the horizontal positions, where they were located in the case of stagnant liquid flow. Figure 11 illustrates the evolution in the bubbly flow structure during a pulsation in the liquid flow by the used dosing pump. At t = 9 s the pulsation by the pump is initiated. At t = 10.8 s a considerable displacement to the left is seen for the adherence and bubble diffusion regions, whereas the bulk region, and hence the large bubbles, appears unaffected by the pulsating liquid flow. The significant difference in time between the two frames is explained by the delay in time between the initiated pulsation of the pump and its influence on the bubbly flow structure is observed. At t = 12.5 s a similar bubbly flow structure as at t = 9 s is observed, after which the periodic cycle reoccurs at a frequency approximately equal to the stroke frequency of the dosing pump. The pulsating liquid flow thus creates a sideways displacement of the bubbly flow structure evolving at the cathode. This displacement of the bubbly flow structure makes the differentiation between the three bubble regions difficult, and furthermore causes mixing of the bubble diameters. Hence, due to a larger production of small bubbles compared to large bubbles the mean bubble diameter is favoured towards that of the small bubbles.

The time averaging of the pulsating liquid flow is seen to indicate a stable mean of the bubble diameter for all horizontal positions. This is further verified by the visualisation of the displacement of the three regions in the bubbly flow structure and mixing of the bubble diameters, shown in Fig. 11. Hence, the displacement of specific bubble diameters could be further investigated by synchronising the camera with the pulsation period of the dosing pump. Thus, the same mean bubble diameters are expected to be acquired at increased horizontal positions compared to the stagnant liquid flow. The current investigations were carried out at one current density as well as with electrodes of a certain size. Further investigations could be conducted at varying current density, which are expected to show an increase in bubble diameter at increasing current density, as reported by Refs. [3, 6, 7, 8]. Similarly, more investigations could be performed with electrodes of decreasing and increasing height. Such investigations are expected to show bubbles with decreasing and increasing diameter, respectively, since bubbles have been observed to increase along the electrode surface due to coalescence with other bubbles and/or mass transfer from supersaturated zones in the liquid phase to the bubbles [6, 8].

5. Conclusion

The aim of this study has been to investigate the three bubble regions reported in the literature: adherence, bubble diffusion and bulk region, under the influence of a pulsating flow. To clearly isolate the effect of the pulsation, a reference investigation at stagnant liquid flow has been performed as well. These investigations have been done using an undivided electrochlorination cell and a Telecentric Direct Image Method (TDIM).

The applied TDIM was verified using polyamid particles of a known mean size of 50 μm. The verification showed that the ap-
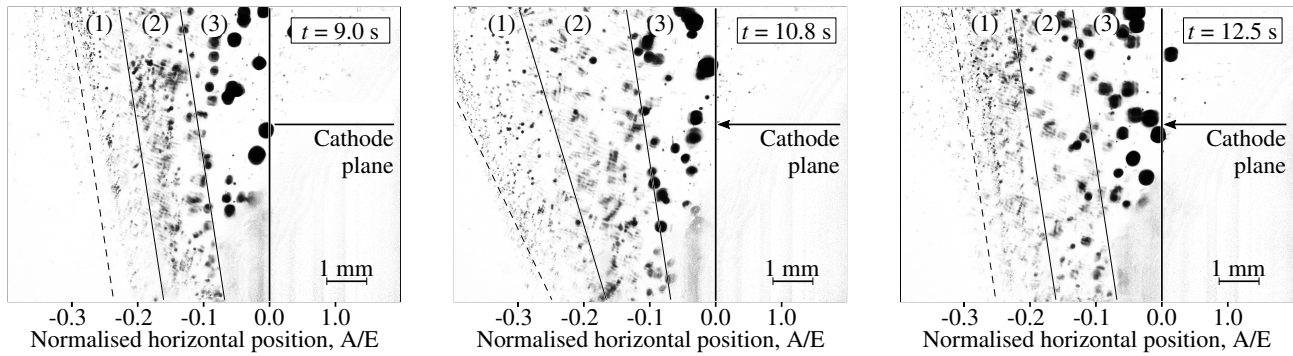
Figure 11: Displacement of the three bubble regions for sequentially captured images during one pulsation period of the dosing pump. Regions: (1) adherence, (2) bubble diffusion, (3) bulk.

plied method estimates a mean size of the polyamid particles of 49.7 µm and thus the TDIM is found applicable for determination of bubble shape and diameter.

The three bubble regions reported to be occurring in bubbly flows are identified: adherence, bubble diffusion and bulk region. The bubble diameter is observed to increase moving from the adherence region to the bulk region.

For stagnant liquid flow it is found that the mean bubble diameter significantly increases with increasing horizontal position in the electrochlorination cell. Furthermore, the fraction of total gas volume for small and large bubbles is found to decrease and increase, respectively, as the horizontal position increases. This is in agreement with the observed increase in bubble diameter across the bubbly flow structure.

For pulsating liquid flow only small variations in mean bubble diameter are observed with increasing horizontal position. Moreover, the pulsating liquid flow shows a more uniform distribution in fraction of total gas volume across different bubble diameters at different positions, which likewise supports the small variations in mean bubble diameter for pulsating liquid flow. The pulsating liquid flow, created by the applied dosing pump, is seen to displace the bubble regions horizontally. Hence, making the differentiation of the three different bubble regions difficult as well as causing mixing of the bubble diameters. This is due to a larger production of small bubbles compared to large bubbles as well as the time averaging resulting from the test methodology, thus favouring the mean diameter towards that of the small bubbles.

6. Acknowledgements

References

[1] Spasojević, M., Krstajić, N., Spasojević, P. and Ribic-Zelenović, L., Modelling current efficiency in an electrochemical hypochlorite reactor, *Chem. Eng. Res. Des.*, 93, pp. 591-601, 2015.

[2] Cheng, C. and Kelsall, G., Models of Hypochlorite production in electrochemical reactors with plate and porous anodes, *J. Appl. Electrochem.*, 37, pp. 1203-1217, 2007.

[3] Dedigama, I., Angeli, P., Ayers, K., Robinson, J., Shearing, P., Tsaoulidis, D. and Brett, D., In situ diagnostic techniques for characterisation of polymer electrolyte membrane water electrolysers - Flow visualisation and electrochemical impedance spectroscopy, *Int. J. Hydrogen Energy*, 39, pp. 4468-4482, 2014.

[4] Aldas, K., Pehlivanoglu, N. and Mat, M., Numerical and experimental investigation of two-phase flow in an electrochemical cell, *Int. J. Hydrogen Energy*, 33, pp. 3668-3675, 2008.

[5] El-Askary, W., Sakr, I., Ibrahim, K. and Balabel, A., Hydrodynamics characteristics of hydrogen evolution process through electrolysis: Numerical and experimental studies, *Energy*, 90, pp. 722-737, 2015.

[6] Boissonneau, P. and Byrne, P., An experimental investigation of bubble-induced free convection in a small electrochemical cell, *J. Appl. Electrochem.*, 30, pp. 767-775, 2000.

[7] Nagai, N., Takeuchi, M. and Nakao, M., Effects of Generated Bubbles Between Electrodes on Efficiency of Alkaline Water Electrolysis, *JSME Int. J.*, 46, pp. 549-556, 2003.

[8] Abdelouahed, L., Hreiz, R., Valentin, G., Poncin, S. and Lapicque, F., Hydrodynamics of gas bubbles in the gap of lantern blade electrodes without forced flow of electrolyte: Experiments and CFD modelling, *Chem. Eng. Res. Des.*, 111, pp. 255-265, 2014.

[9] Dedigama, I., Angeli, P., Dijk, N., Millichamp, J., Shearing, P., Tsaoulidis, D. and Brett, D., Current density mapping and optical flow visualisation of a polymer electrolyte membrane water electrolyser, *J. Power Sources*, 265, pp. 97-103, 2014.

[10] Li, D. and Tian, J., An accurate calibration method for a camera with telecentric lenses, *Optics and Lasers in Engineering*, 51, pp. 538-541, 2013.

[11] Chaira, T., Ray, A.K., *Fuzzy Image Processing and Applications with MATLAB*, first ed., CRC Press, Florida, 2010.